Near-field mapping of the edge mode of a topological valley slab waveguide at λ = 1.55 μm

Alexander M. Dubrovkin[1,2*], Udvas Chattopadhyay[2], Bo Qiang[1,3], Oleksandr Buchnev[4], Qi Jie Wang[1,2,3], Yidong Chong[1,2*], and Nikolay I. Zheludev[1,2,4*]

[1]*Centre for Disruptive Photonic Technologies, TPI, Nanyang Technological University, 637371 Singapore*

[2]*School of Physical and Mathematical Sciences, Nanyang Technological University, 637371 Singapore*

[3]*Centre for OptoElectronics and Biophotonics, School of Electrical and Electronic Engineering, Nanyang Technological University, 639798 Singapore*

[4]*Optoelectronics Research Centre and Centre for Photonic Metamaterials, University of Southampton, SO17 1BJ, UK*

*e-mail: dubrovkin@ntu.edu.sg, yidong@ntu.edu.sg, niz@orc.soton.ac.uk

ABSTRACT

Valley polarized topological states of light allow for robust waveguiding which has been demonstrated for transverse-electric modes in THz and near-infrared parts of the spectrum. As the topological protection relies on guiding the light via a highly structured surface, direct imaging of the photonic modes at sub-unit cell resolution is of high interest but challenging in particular for transverse-magnetic modes. Here, we report mapping the transverse-magnetic modes in a valley photonic crystal waveguide using scattering-type scanning near-field optical microscopy at the optical telecom C-band wavelength. The waveguide based on a triangular air-hole motif with broken inversion symmetry is fabricated from suspended Germanium layer. We observed the launching and guiding of the transverse-magnetic edge mode along the boundary between topologically distinct domains with opposite valley Chern indices. These results are supported by theoretical simulations, and provide insight into the design and use of topological protected states for applications in densely integrated optical telecommunication devices.

Integrated waveguides are a key technology in on-chip photonics.[1] They enable optical interconnects for optoelectronic circuits and information processing chips. Since early works utilizing the principle of total internal reflection in dielectrics,[2,3] several alternative approaches have been developed to address the demand for unperturbed light propagation and miniaturization of photonic circuits. These include the implementation of advanced concepts in the structuring of dielectrics (e.g. photonic crystals[4-6] and subwavelength integrated photonics[7]), as well as the use of plasmonic[8] and other advanced materials.[9,10] Although the latter approach holds considerable potential for making arbitrarily-shaped[11] and compact[12-16] waveguides, its applicability remains limited due to considerable optical losses. The use of appropriately structured dielectrics, on the other hand, enables both compact designs and long-range light propagation. Photonic crystal waveguides allow high transmission through sharp bends,[17] which significantly reduces device footprints compared to conventional ridge-based architecture.

This advantage has been developed even further with the invention of topological photonics,[18-20] which allows for topologically protected edge states that support one-way light propagation. These photonic modes require the realization of a photonic topological insulator – a medium performing as an insulator in the bulk while hosting propagating states along its edges as a result of nontrivial topology in the photonic band structure. This class of waveguides was initially realized in the microwave domain using photonic crystals made of magnetically-biased gyromagnetic materials.[21] Subsequent works developed alternative routes to achieving photonic topological edge states without magnetic materials, e.g. by using specially-designed photonic crystals with broken inversion symmetry,[22-37] thus enabling topological waveguiding in a broader range of the electromagnetic spectrum. Valley photonic

crystal (VPC) waveguides – a realization of this approach based on the emulation of the valley Hall effect – has shown particularly high promise for all-dielectric on-chip photonics in the telecom[38] and terahertz[39] spectral range. VPCs can be implemented as honeycomb crystal lattices with C_3 symmetry in each unit cell, on a high-index semiconductor slab platform. VPC-based topological waveguides support propagating edge states inside the light cone, which have been studied via detection of transmitted radiation. However, the direct imaging of light flow in a VPC slab waveguides at optical frequencies remains unexplored, due to the challenge of subwavelength-scale field imaging in photonic crystals. In this work, we introduce the use of scattering-type scanning near-field optical microscopy (s-SNOM)[40] to directly map VPC waveguides supporting transverse-magnetic (TM) topological modes in the telecom range.

The VPC used in this work is based on a triangular air-hole motif with broken inversion symmetry, following a complementary design to the photonic valley Hall structure introduced in Ref.[23] (i.e. pillars are replaced with holes). This photonic crystal structure supports topologically protected TM edge modes, which can be particularly relevant for on-chip topological lasing applications.[41] The topological features arise from the concentration of Berry curvature in the corners of the first Brillouin zone,[25,42] as demonstrated in the 2D finite element calculation results plotted in Fig. 1(a). The actual experimental structure implemented in our work is based on a suspended semiconductor slab consisting of a high-index functional layer (germanium) and a low-index supporting membrane (silicon nitride). Ge films were fabricated by thermal deposition in high vacuum (10^{-7} mTorr base pressure) using a Univex 250 system (Leybold); commercially available Si_3N_4 membranes, suspended over a window in a bulk silicon frame, were obtained from Norcada.

A schematic of the slab-VPC's unit cell is shown in Fig. 1(b) (black and blue colours indicate Ge and Si_3N_4 respectively). We optimized the periodic honeycomb structure by varying the strength of the inversion symmetry breaking (represented by d_1, d_2), the crystal period, and the germanium thickness. A band structure for the resulting design, intended for operation in the telecom range and feasible for the fabrication, is plotted in Fig. 1(c). The TM-like topological band gap is highlighted in yellow. The corresponding slab structure consists of a germanium layer and silicon nitride membrane of 260 nm and 100 nm thicknesses respectively. To fabricate the VPC, we used focus ion beam milling (FIB) in a Helios NanoLab 650 system (FEI). Triangular holes were completely etched through the Ge layer; the thin Si_3N_4 membrane was left only partially perforated to enable a flat surface on one side of the structured slab. A scanning electron microscopy (SEM) image of a typical photonic crystal fabricated by this process is shown in Fig. 1(d).

In the past decade, s-SNOM has been used to map a wide variety of nanoscale waveguide modes, benefiting from its wavelength-independent optical resolution, extending down to the 10 nm scale.[12-16,43,44] Since the technique is based on atomic-force microscopy combined with the tip-scattered light detection, it requires relatively flat surfaces for correct operation. To account for this, we perform the experiment using the configuration schematically illustrated in Fig. 2(a). The Ge layer is fabricated on the bottom side of the membrane, i.e. inside the supporting frame (not shown), while the near-field measurements are carried out on the flat top surface of the device. We use a commercial transmission-mode s-SNOM setup (Neaspec), which operates at 1.55 um laser wavelength and maintains a synchronized sample-illumination regime. In this mode, the illumination spot is kept at the same position on the sample during the scanning process.[44] Laser radiation is focused at a slit (with orthogonal polarization) that launches a plane-wave-like TM mode in the unpatterned area of the slab.

This mode excites the topological waveguide structure, which is mapped by the s-SNOM tip (Arrow-NCPt (Nanoworld), with ~245-275 kHz oscillation frequency) via a pseudo-heterodyne detection scheme. A bottom-view SEM image depicting a typical experimental configuration of the slit launcher and the topological waveguide structure is shown in Fig. 2(c). We utilize the tip-scattered signal demodulated at the second (s_2) harmonic of the tip oscillation frequency, and the vertically polarized component of the tip-scattered light is selected using a polarizer.

To construct the topological waveguide, we combine two VPCs with opposite valley Chern indices by flipping the orientation of the triangular air holes in one crystal with respect to the other. An SEM image of such a structure is shown in Fig. 2(d), where the two topologically distinct domains are highlighted in red and yellow. This configuration enables topological waveguiding in a frequency range corresponding to the bulk band gap of the VPC, by means of edge states at the boundary between the topologically distinct domains. A 3D numerical simulation (via COMSOL) of topological waveguiding (optimized for transmission via topological edge state) is shown in Figs. 2(b) and S1 (supplementary material). In this simulation, the excitation of the photonic structure (from the right-hand side to the left) was accomplished using a rectangular port mimicking the slit-launcher used in the experiment. The resulting field distribution indicates that the proposed platform provides suitable conditions for coupling into and transmitting along the VPC waveguide. The waveguide mode is strongly confined to the interface between the distinct VPC domains.

Figure 3(a) shows an experimentally-obtained s-SNOM image of light propagation through the optimized VPC waveguide. The propagation direction is from the right to the left. The structure performs as a spatial filter, enabling transmission of the incident light through the

center channel (i.e. the boundary between topologically distinct domains), which is relevant to microwave near-field experiments[24,25,29,45] and far-field observations on various slab topological platforms.[27,33,35,46] Some of the incident light is coupled into the bulk VPC domains, but these mode intensities decay significantly with propagation distance, whereas the mode confined to the topological interface remains clearly visible. We observe that the waveguide mode is confined to within 1.4 um of the domain wall (Fig. 3(b)), estimated as the width at half maximum of a Lorentzian profile (blue curve) fitted to the averaged vertical cross-section of the measured near field intensity (black curve). The light transmitted via the interface outcouples at the opposite end of the VPC, and thereafter diverges into the unstructured slab on the left side of the structure.

To find the VPC waveguides with the best waveguiding features in the actual experiments, we systematically explored structures with different lattice constants, using the theoretically optimized value as a reference starting point. The s-SNOM measurements were used to identify the optimized design supporting high confinement and transmission via the edge mode. All experimental measurements were carried out at the same excitation wavelength defined by the single-frequency source of the s-SNOM apparatus. We found the optimized experimental lattice constant to be shifted to larger values compared to the theoretical estimate, which may be ascribed to discrepancies between the materials parameters of the real materials and the simulation models and deviations of the fabricated structure geometry compared to the nominal shape. An example of s-SNOM mapping over an off-tuned VPC waveguide is shown in Fig. 3(c). The structure has the same number of unit cells as the optimized waveguide, and appears smaller in size due to the reduced lattice constant. In this case, the light propagation is spread over the whole region of the top and bottom VPC domains, without any enhanced transmission though the center channel. The measured

intensity profile shows no strong central peak (Fig. 3(d)), unlike the sharp peak seen in Fig. 3(b).

In summary, we have performed near-field optical mapping of a two-dimensional topological photonic structure using scattering-type scanning near-field optical microscopy in the telecom frequency range. The topological waveguide is hosted in a valley photonic crystal waveguide specifically designed to support a topological gap in the transverse magnetic spectrum with a suspended slab geometry, which enables near-field imaging on the flat side of the membrane. We have directly observed the coupling of light from the unpatterned slab medium into a guided mode in the topological photonic crystal structure. The observed strong confinement of the optical field along the interface between topologically distinct domains, which have opposite valley Chern indices, agrees with theoretical predictions. The outcoupling of light from the topological waveguide occurs from a small area where the topological interface terminates. This work provides a pathway for nanoscale imaging of waveguiding in topological nanophotonic structures. Although the present experiments were done at telecom frequencies, similar near-field techniques can achieve deeply nanoscale resolutions, and thus can be potentially applied to topological waveguides operating in the visible range.

See the supplementary material for additional simulation of the light propagation through bended VPC waveguide.

Following a period of embargo, the data from this paper can be obtained from the University of Southampton ePrints research repository, https://doi.org/10.5258/SOTON/XXXXX.

This research was supported by the Singapore Ministry of Education Academic Research Fund MOE2016-T3-1-006 (S), by the National Research Foundation Singapore programme NRF-CRP18-2017-02 and NRF–CRP19–2017–01, and by the UK Engineering and Physical Sciences Research Council [Grant EP/M009122/1].

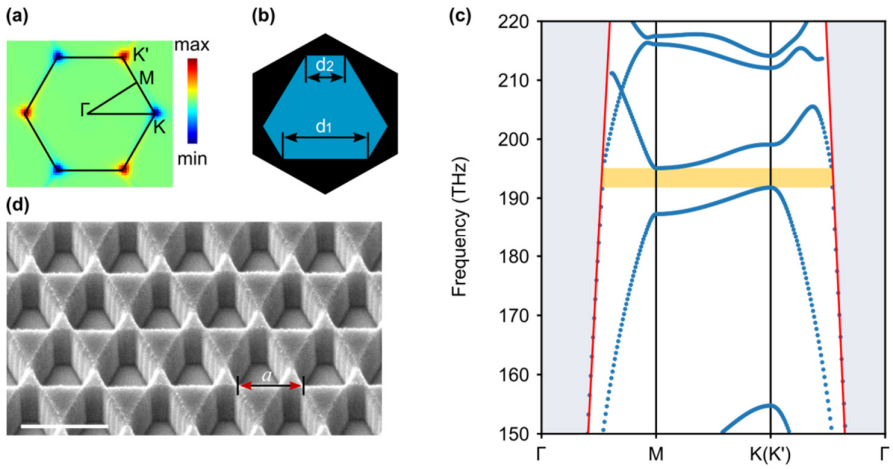

Fig. 1. Design of the valley photonic crystal (VPC). (a) Distribution of the Berry curvature in the first Brillouin zone. (b) Schematic of the slab-VPC's unit cell; black and blue colors represent the germanium layer and the silicon nitride supporting membrane respectively. (c) Band structure of the VPC calculated for a 260 nm thick lossless Ge layer on 100 nm thick half-perforated Si_3N_4 slab, with parameters a = 470 nm, $d_1 = 0.6a$ and $d_2 = 0.26a$. The TM-like gap is highlighted in yellow. (d) SEM tilted-view image of a typical VPC fabricated by FIB milling. The scale bar is 1 μm, and the arrow indicates one period (a) of the crystal.

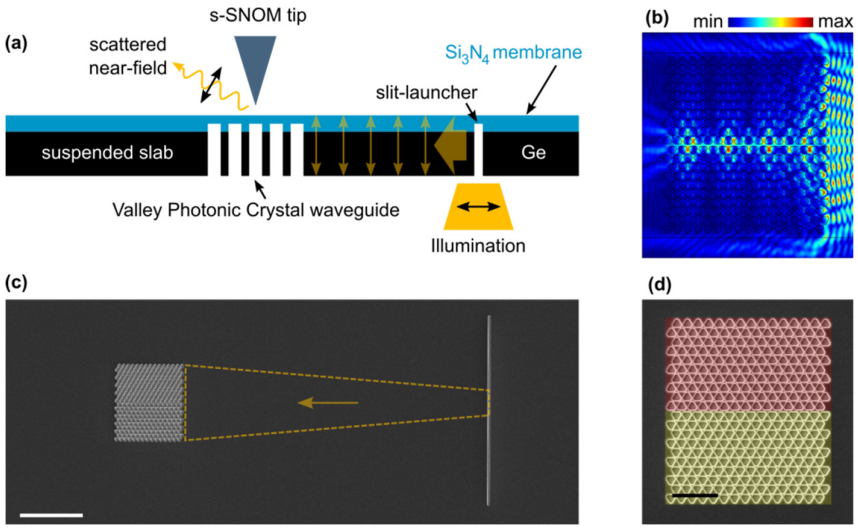

Fig. 2. Launching and mapping light in VPC waveguides. (a) Schematic of the nanoimaging experiment. (b) Simulated TM polarized field profile showing transmission through the waveguide, calculated for a 260 nm thick lossless Ge layer on a 100 nm thick half-perforated Si_3N_4 slab at 193.5 THz, with a = 470 nm, $d_1 = 0.6a$, and $d_2 = 0.26a$; the colour bar corresponds to the magnitude of the vertical component of electric field in the middle of the slab. (c) SEM bottom-view image of a typical experimental sample; the yellow marks depict the part of slit-launched light propagating to the VPC waveguide; the scale bar is 10 μm. (d) SEM image of a typical VPC structure consisting of two topologically-distinct domains with opposite valley Chern indices (highlighted with red and yellow pseudo colours); the scale bar is 3 μm.

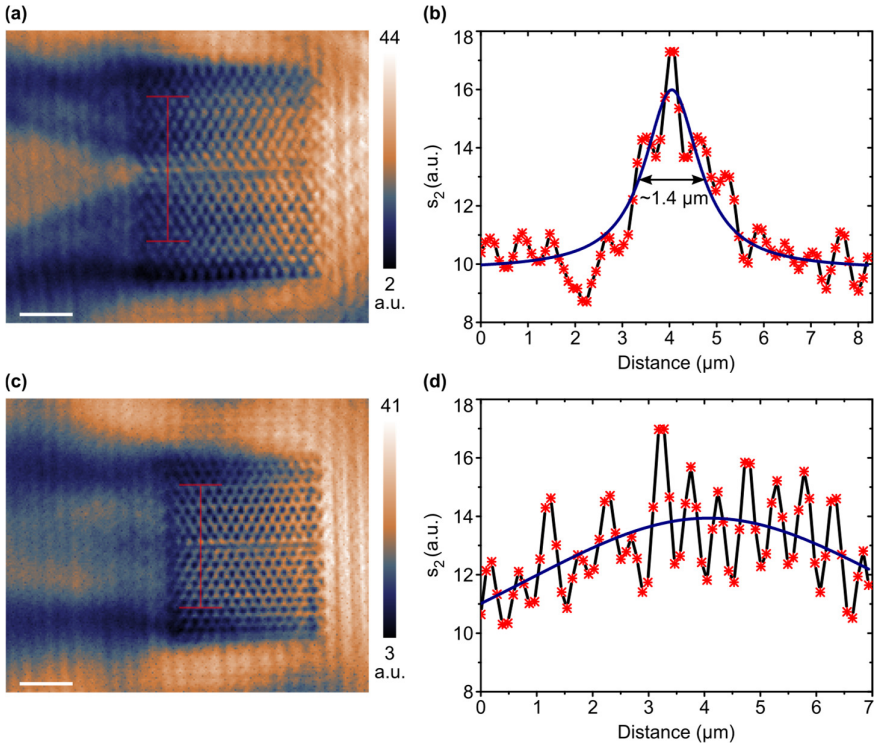

Fig. 3. s-SNOM mapping of VPC waveguides. (a) Near-field distribution (optical amplitude s_2) for the structure with period a = 711 nm. (b) The corresponding vertical cross-section (black curve), averaged along the region marked in red in subplot (a); blue curve is the best fit Lorentzian profile. (c) and (d) Near-field distribution and averaged cross-section for the structure with period a = 613 nm. Averaging is performed based on 25 adjacent vertical lines in the sampling region. Scale bars in panels (a) and (c) are 3 μm.

REFERENCES

[1]A. H. Atabaki, S. Moazeni, F. Pavanello, H. Gevorgyan, J. Notaros, L. Alloatti, M. T. Wade, C. Sun, S. A. Kruger, H. Meng, K. Al Qubaisi, I. Wang, B. Zhang, A. Khilo, C. V. Baiocco, M. A. Popović, V. M. Stojanović, and R J. Ram, Nature **556**, 349 (2018).

[2]R. A. Soref and J. P. Lorenzo, Electron. Lett. **21**, 953 (1985).

[3]R. A. Soref and J. P. Lorenzo, IEEE J. Quantum Electron, **QE-22**, 873 (1986).

[4]E. Yablonovitch, Phys. Rev. Lett. **58**, 2059 (1987).

[5]S. John, Phys. Rev. Lett. **58**, 2486 (1987).

[6]J. D. Joannopoulos, S. G. Johnson, J. N. Winn, and R. D. Meade, *Photonic Crystals: Molding the Flow of Light*, 2nd ed. (Princeton University Press, New Jersey, 2008).

[7]P. Cheben, R. Halir, J. H. Schmid, H. A. Atwater, and D. R. Smith, Nature **560**, 565 (2018).

[8]R. Zia, J. A. Schuller, A. Chandran, M. L. Brongersma, Mater. Today **9**, 20 (2006).

[9]D. N. Basov, M. M. Fogler, and F. J. García de Abajo, Science **354**, aag1992 (2016).

[10]T. Low, A. Chaves, J. D. Caldwell, A. Kumar, N. X. Fang, P. Avouris, T. F. Heinz, F. Guinea, L. Martin-Moreno, and F. Koppens, Nat. Mater. **16**, 182 (2017).

[11]I. Liberal and N. Engheta, Nat. Photon. **11**, 149 (2017).

[12]J. Chen, M. Badioli, P. Alonso-González, S. Thongrattanasiri, F. Huth, J. Osmond, M. Spasenović, A. Centeno, A. Pesquera, P. Godignon, A. Z. Elorza, N. Camara, F. J. García de Abajo, R. Hillenbrand, and F. H. L. Koppens, Nature **487**, 77 (2012).

[13]Z. Fei, A. S. Rodin, G. O. Andreev, W. Bao, A. S. McLeod, M. Wagner, L. M. Zhang, Z. Zhao, M. Thiemens, G. Dominguez, M. M. Fogler, A. H. Castro Neto, C. N. Lau, F. Keilmann, and D. N. Basov, Nature **487**, 82 (2012).

[14]S. Dai, Z. Fei, Q. Ma, A. S. Rodin, M. Wagner, A. S. McLeod, M. K. Liu, W. Gannett, W. Regan, K. Watanabe, T. Taniguchi, M. Thiemens, G. Dominguez, A. H. Castro Neto, A.

Zettl, F. Keilmann, P. Jarillo-Herrero, M. M. Fogler, and D. N. Basov, Science **343**, 1125 (2014).

[15]A. M. Dubrovkin, B. Qiang, H. N. S. Krishnamoorthy, N. I. Zheludev, and Q. J. Wang, Nat. Commun. **9**, 1762 (2018).

[16]Z. Fei, M. E. Scott, D. J. Gosztola, J. J. Foley IV, J. Yan, D. G. Mandrus, H. Wen, P. Zhou, D. W. Zhang, Y. Sun, J. R. Guest, S. K. Gray, W. Bao, G. P. Wiederrecht, and X. Xu, Phys. Rev. B **94**, 081402(R) (2016).

[17]A. Mekis, J. C. Chen, I. Kurland, S. Fan, P. R. Villeneuve, and J. D. Joannopoulos, Phys. Rev. Lett. **77**, 3787 (1996).

[18]L. Lu, J. D. Joannopoulos, and M. Soljačić, Nat. Photon. **8**, 821 (2014).

[19]A. B. Khanikaev and G. Shvets, Nat. Photonics **11**, 763 (2017).

[20]T. Ozawa, H. M. Price, A. Amo, N. Goldman, M. Hafezi, L. Lu, M. C. Rechtsman, D. Schuster, J. Simon, O. Zilberberg, and I. Carusotto, Rev. Mod. Phys. **91**, 015006 (2019).

[21]Z. Wang, Y. Chong, J. D. Joannopoulos, and M. Soljačić, Nature **461**, 772 (2009).

[22]L.-H. Wu and X. Hu, Phys. Rev. Lett. **114**, 223901 (2015).

[23]T. Ma, and G. Shvets, New J. Phys. **18**, 025012 (2016).

[24]Y. Yang, Y. F. Xu, T. Xu, H.-X. Wang, J.-H. Jiang, X. Hu, and Z. H. Hang, Phys. Rev. Lett. **120**, 217401 (2018).

[25]X. Wu, Y. Meng, J. Tian, Y. Huang, H. Xiang, D. Han, and W. Wen, Nat. Commun. **8**, 1304 (2017).

[26]S. Barik, A. Karasahin, C. Flower, T. Cai, H. Miyake, W. DeGottardi, M. Hafezi, and E. Waks, Science **359**, 666 (2018).

[27]M. A. Gorlach, X. Ni, D. A. Smirnova, D. Korobkin, D. Zhirihin, A. P. Slobozhanyuk, P. A. Belov, A. Alù, and A. B. Khanikaev, Nat. Commun. **9**, 909 (2018).

[28]X.-D. Chen, F.-L. Zhao, M. Chen, and J.-W. Dong, Phys. Rev. B **96**, 020202 (2017).

[29]F. Gao, H. Xue, Z. Yang, K. Lai, Y. Yu, X. Lin, Y. Chong, G. Shvets, and B. Zhang, Nat. Phys. **14**, 140 (2018).

[30]J. Noh, S. Huang, K. P. Chen, and M. C. Rechtsman, Phys. Rev. Lett. **120**, 063902 (2018).

[31]Y. Kang, X. Ni, X. Cheng, A. B. Khanikaev, and A. Z. Genack, Nat. Commun. **9**, 3029 (2018).

[32]P. D. Anderson and G. Subramania, Opt. Express **25**, 23293 (2017).

[33]N. Parappurath, F. Alpeggiani, L. Kuipers, and E. Verhagen, Sci. Adv. **6**, eaaw4137 (2020).

[34]S. Peng, N. J. Schilder, X. Ni, J. van de Groep, M. L. Brongersma, A. Alù, A. B. Khanikaev, H. A. Atwater, and A. Polman, Phys. Rev. Lett. **122**, 117401 (2019).

[35]D. Smirnova, S. Kruk, D. Leykam, E. Melik-Gaykazyan, D.-Y. Choi, and Y. Kivshar, Phys. Rev. Lett. **123**, 103901 (2019).

[36]X.-T. He, E.-T. Liang, J.-J. Yuan, H.-Y. Qiu, X.-D. Chen, F.-L. Zhao, and J.-W. Dong, Nat. Commun. **10**, 872 (2019).

[37]J.-W. Dong, X.-D. Chen, H. Zhu, Y. Wang, and X. Zhang, Nat. Mater. **16**, 298 (2017).

[38]M. I. Shalaev, W. Walasik, A. Tsukernik, Y. Xu, and N. M. Litchinitser, Nat. Nanotech. **14**, 31 (2019).

[39]Y. Yang, Y. Yamagami, X. Yu, P. Pitchappa, J. Webber, B. Zhang, M. Fujita, T. Nagatsuma, and R. Singh, Nat. Photon., https://doi.org/10.1038/s41566-020-0618-9 (2020).

[40]F. Keilmann and R. Hillenbrand, Phil. Trans. R. Soc. Lond. A **362**, 787 (2004).

[41]Y. Zeng, U. Chattopadhyay, B. Zhu, B. Qiang, J. Li, Y. Jin, L. Li, A. G. Davies, E. H. Linfield, B. Zhang, Y. Chong, and Q. J. Wang, Nature **578**, 246 (2020).

[42]T. Fukui, Y. Hatsugai, and H. Suzuki, J. Phys. Soc. Jpn. **74**, 1674 (2005).

[43]R. Hillenbrand and F. Keilmann, Appl. Phys. Lett. **80**, 25 (2002).

[44]V. A. Zenin, A. Andryieuski, R. Malureanu, I. P. Radko, V. S. Volkov, D. K. Gramotnev, A. V. Lavrinenko, and S. I. Bozhevolnyi, Nano Lett. **15**, 8148 (2015).

[45]A. Slobozhanyuk, A. V. Shchelokova, X. Ni, S. H. Mousavi, D. A. Smirnova, P. A. Belov, A. Alù, Y. S. Kivshar, and A. B. Khanikaev, Appl. Phys. Lett. 114, 031103 (2019).

[46]A. Vakulenko, S. Kiriushechkina, M. Li, D. Zhirihin, X. Ni, S. Guddala, D. Korobkin, A. Alù, and A. B. Khanikaev, preprint arXiv:1911.11110 (2019).